Simulation of high brightness tapered lasers

I. Esquivias*[a], H. Odriozola[a], J. M.G. Tijero[a], L. Borruel[a], A. M. Mínguez[a], N. Michel[b], M. Calligaro[b], M. Lecomte[b], O. Parillaud[b], and M. Krakowski[b]

[a]Universidad Politécnica de Madrid, ETSI Telecomunicación, Madrid 28040, Spain
[b]Alcatel-Thales III-V Lab, Route Départementale 128, 91767 Palaiseau, France

ABSTRACT

Tapered semiconductor lasers have demonstrated both high power and good beam quality, and are of primary interest for those applications demanding high brightness optical sources. The complex non-linear interaction between the optical field and the active material requires accurate numerical simulations to improve the device design and to understand the underlying physics. In this work we present results on the design and simulation of tapered lasers by means of a Quasi-3D steady-state single-frequency model. The results are compared with experiments on Al-free active region devices emitting at 1060 nm. The performance of devices based on symmetric and asymmetric epitaxial designs is compared and the influence of the design on the beam properties is analyzed. The role of thermal effects on the beam properties is experimentally characterized and analyzed by means of the numerical simulations. Tapered lasers with separate electrical contacts in the straight and tapered sections, based on symmetrical and asymmetrical epitaxial designs are also presented and analyzed.

Keywords: Semiconductor lasers, High brightness lasers, tapered lasers, modeling, simulation, thermal effects

1. INTRODUCTION

Laser applications requiring high power coupled into an optical fiber demand high brightness sources at specific wavelengths. Tapered semiconductor lasers[1-3], also known as flared unstable cavity lasers, are a cost-effective solution which has demonstrated both high power and good beam quality. These devices consist of a ridge waveguide (RW) section and a tapered section (see Fig. 1). The single spatial mode of the RW section is launched into the tapered section where it is amplified while keeping its single mode profile. Gain guided tapered single emitters with a taper angle close to the free diffraction angle have demonstrated good beam quality and output powers between 2 and 5 W at different wavelengths (see 2,3 and references herein). Improved epitaxial structures, together with the use of long cavity designs have led to single-emitter tapered lasers providing more than 10 W with a low beam propagation ratio M^2 at 980 nm[4] and 1060 nm[3].
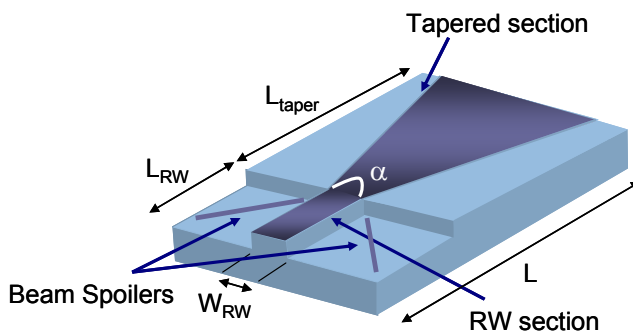

Fig. 1 Schematics of a gain guided tapered laser.

It is well known that the interaction between the optical field and the semiconductor gain media promotes a complex spatial-spectral dynamics in semiconductor lasers. In the case of tapered lasers, non-linear effects, such as Spatial Hole Burning (SHB) and thermal lensing add complexity to the physical phenomena involved. Efficient and accurate modeling approaches are thus necessary to analyze and predict the beam properties of tapered lasers in order to design new geometries with improved performance.

*esquivia@tfo.upm.es; phone +34 91 3367339; fax +34 91 3367319;

Our group at the Universidad Politécnica of Madrid, in collaboration with the University of Nottingham, has developed a sophisticated simulator for tapered lasers[5-7], called CONAN, which solves the electrical, optical and thermal equations for these devices. Despite the assumptions needed to reduce the model complexity (steady state, single frequency, two-dimensional propagation of the optical mode), the simulations have shown good qualitative and quantitative agreement with experimental results in tapered lasers with different geometries and based on different materials[6-8]. Furthermore, the simulator has demonstrated to be a useful tool to predict the behavior of novel designs prior to their fabrication[9-10]. Other models in literature[11-12], based on similar approaches, have also reproduced the main trends observed experimentally.

In this work, we present a comprehensive summary of our simulation model together with recent modelling results in comparison with experiments performed in 1060 nm devices. In particular we present results on tapered lasers based on asymmetric epitaxial designs, analyze the role of thermal effects in gain guided tapered lasers, and discuss the role of the epitaxial design on the performance of tapered lasers with separate contacts.

2. SIMULATION MODEL

2.1 Description of model basis

Our initial quasi-3D model for tapered lasers has been reported in detail[5-7], and therefore only basic features are described here. In brief, the complete steady state electrical, thermal, and optical equations for the tapered laser are solved self-consistently, assuming a single frequency. The laser simulator includes a 3D electrical solver of the Poisson and continuity equations coupled to a 3D thermal solver of the heat-flow equation with the local heat sources provided by the electrical solution. The solution procedure is initialized by a 1-D laser simulator (HAROLD 3.0[13]) which provides for each bias current the lasing wavelength, the bias voltage, and the average photon density in the laser cavity.

Table 1: Main physical effects included in the model

Physical Effect or Parameter	Included	Comments
Temperature dependence of energy gap	YES	Empirical Varshni form
Bang gap renormalization	NOT	
Contribution to current density from thermal gradients	YES	Defined by the electron and hole thermoelectric powers
Carrier capture/escape processes in the QW	YES	Defined by electron and hole capture times
Thermionic emission in heterojunctions	NOT	
Fermi-Dirac statistics in bulk materials	NOT	
Dependence of electron and hole mobilities on dopant concentration	YES	Electric field and temperature dependencies not included
Auger recombination	YES	Temperature dependent Auger parameters
Shockley-Read-Hall (SRH) non-radiative recombination	YES	Complete SRH formula, dependent on both electron and hole carrier concentrations, and on trap properties (density, energy and degeneration factor of the trap, considering a temperature dependent capture cross section)
Wavelength dependence of refractive index	YES	Temperature dependence not included
Free carrier absorption	YES	Linear with local carrier concentration, defined by electron and hole free carrier absorption coefficients
Non-constant Linewidth Enhancement Factor	YES	Calculated in QW region from a carrier dependent differential refractive index, and carrier and wavelength dependent differential gain
Gain broadening	YES	Lorentzian function
Coulomb enhancement of the gain	NOT	
Spontaneous emission noise	NOT	
Detailed calculation of local heat sources	YES	Local heat sources: Joule effect, non-radiative recombination, free-carrier absorption
Temperature dependence of thermal conductivities	YES	Included in semiconductor layers

The tapered laser is divided into two-dimensional (2D) slices perpendicular to the cavity axis. The 1-D average photon density is used to define an initial guess optical field at the first slice, in the rear facet of the device. The photon density of this field is used as input for the electro-thermal solver to calculate the lateral gain and refractive index perturbation profiles in the first slice. With these inputs, a 2D-Wide Angle Finite Difference Beam Propagation Method (BPM)

making use of the effective index approximation propagates the optical field through the first slice and provides the electro-thermal solver with the photon density profile corresponding to the next slice. After a number of round trips, a stable optical field distribution, both in shape and power, is found. For the simulation of tapered lasers with separate contacts the model was conveniently modified[8]. The device is divided into as many sections as separate contacts and a different bias voltage is applied to each section. The current through each section is calculated by integration of the resulting current density profile.

The material gain and the spontaneous recombination rate for the considered QW active layer are first calculated as a function of the carrier density using an external band-mixing model. Then, the results are fitted to a parabolic valence band approach, using as fitting parameters the effective masses of the QW levels and two linear correction parameters, one for the gain and the other for the spontaneous recombination rate. The reason for using a parabolic valence band model with fitted parameters was to reduce the computational effort in the 3D simulations. The material parameters employed in the simulations are taken from standard references when properly known or assumed otherwise. Table I summarizes the main physical effects included in the model and how their dependency on temperature, wavelength or carrier densities has been considered.

2.2 Model options regarding symmetry

Three different options are included in the simulator regarding the initially launched field and the symmetry of the propagating field. Our original model[5-7] solves the electrical, thermal and optical equations in half-cavity (HC) to reduce the computational effort, thus assuming a symmetrical solution for the optical field and consequently symmetric solutions for the photon density, carrier density and temperature profiles. Although as initial optical field we usually launch into the rear facet the fundamental mode of the passive RW section, an even function, we have checked that the final optical field is independent of the shape of the initial field, provided it is an even function. This HC model, however, cannot take into consideration the effect of second order odd modes since the BPM preserves the parity of the field. Therefore, model was later extended[14] in order to consider the full cavity and to allow for the possibility of launching an asymmetric field $E_a(x)$, which contains odd and even components, i.e., $E_a(x) = E_e(x) + E_o(x)$. The corresponding photon density used to solve the electrical equations is then calculated using two alternative approaches:

- Full Cavity Coherent Coupling (FCCC): The photon density is taken as proportional to $|E_a(x)|^2$ with $E_a(x)$ being the optical field after the propagation by the BPM through the previous slice. This photon density is in general asymmetric, although it can result in a final symmetric solution, depending on the particular device under study. This case is equivalent to the coherent coupling of even and odd modes.

- Full Cavity Incoherent Coupling (FCIC): The photon density is calculated as proportional to $|E_s(x)|^2$, the addition of the field intensities of the even and odd components of $E_a(x)$: $|E_s(x)|^2 = |E_e(x)|^2 + |E_o(x)|^2$. In this way the photon density is symmetric, and consequently also the carrier and temperature profiles. This approach is equivalent to propagate simultaneously an even and an odd field with slightly different frequencies and therefore only coupled through its interaction with the gain medium, i.e. incoherently coupled.

The different results provided by the three model options are illustrated in Fig. 2, which corresponds to the simulation of a RW laser with a passive waveguide supporting two lateral modes. The top row in Fig. 2 shows the intensity of the forward optical field and the bottom row shows the Near Field (NF) patterns at the facet for different power levels. In the case of the HC model, only the fundamental mode is propagated yielding a symmetric NF at all power levels. The FCCC model produces a snake like intensity profile in the plane of the active layer, which is usually not stable after different roundtrips; the corresponding NF profile is asymmetric and it is shifted with respect to the longitudinal axis. This kind of behavior has been experimentally observed and it was attributed to the coherent coupling of frequency locked lateral modes[15]. The FCIC model produces a symmetric intensity distribution and NF profile: at low power the fundamental mode is dominant but by increasing the power the SHB effect promotes the onset of the second order mode yielding a double peak distribution in the NF and Far Field (FF) profiles.
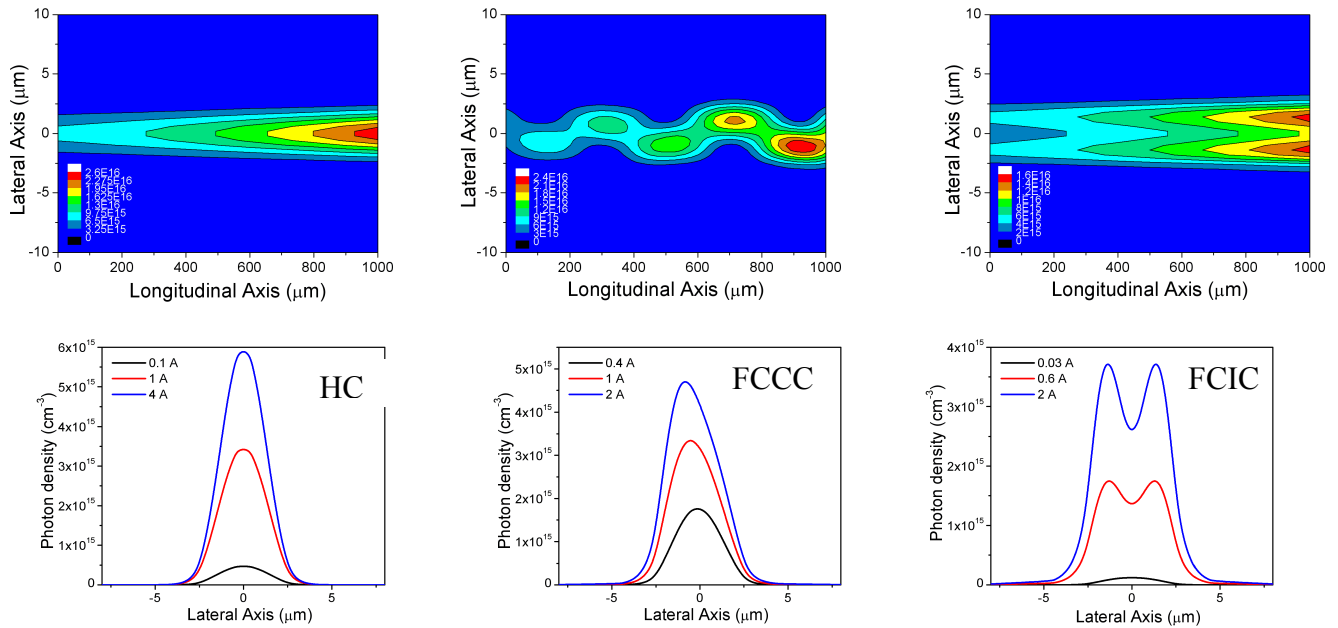
Fig. 2: Simulated intensity of the forward optical field (top) and NF patterns (bottom) for a RW laser calculated using the Half-cavity model (left), Full Cavity Coherent Coupling model (center) and Full Cavity Incoherent Coupling model (right).

3. SIMULATION RESULTS AND COMPARISON WITH EXPERIMENTS

3.1 Tapered lasers based on asymmetric epitaxial structures.

In a previous work[16] we analyzed by means of numerical simulations, the brightness improvement of tapered lasers with asymmetrical epitaxial designs. The basic idea in these designs is to decrease the optical confinement factor Γ (or to increase the ratio d_w/Γ, with d_w being the active layer thickness) in order to reduce the active layer photon density at a given output power. In this way, the onset of the non-linear effects causing deterioration of the beam quality (carrier lensing and self-focusing) is delayed up to a higher optical output power. An additional benefit of asymmetric designs with the QW located close to the p-cladding is the reduction of free-carrier absorption losses and series resistance. The main drawbacks of asymmetric designs are the risk of lasing in secondary transverse modes and the increase of the threshold current. Here we present simulations in comparison with experimental results on 1060 nm gain guided tapered lasers demonstrating the improvement of the beam quality by the use of an asymmetric epitaxial structure.

The laser structure consists of a strained InGaAs QW embedded in a large InGaAsP optical cavity with AlGaAs cladding regions. The asymmetric design (a-SQW) uses an Al content in the n-cladding lower than that in the p-cladding, and the QW is located close to the p-cladding. A symmetric design (s-SQW) was also grown for reference. Gain guided tapered lasers were fabricated with a total cavity length of 3 mm and taper angles of 4º and 6º. Antireflective (AR) and high (HR) reflection coatings were applied to the front and back facet, respectively. The p-side down mounted devices were characterized at room temperature in CW operation. Details on the laser structure and experimental results on devices based on the s-SQW design can be found elsewhere[17].

Fig. 3a) shows the experimental and simulated Power-Current characteristics of 4º tapered lasers based on the s-SQW and a-SQW designs. Those simulation parameters depending on material quality (scattering losses and trap density) or non properly known (refractive index of InGaAsP at 1060 nm) were previously estimated by comparing 1D simulations with experiments in Broad Area lasers[18]. As it can be seen in Fig. 3a), the agreement between experiments and simulations in terms of threshold current and slope efficiency was fairly good, especially taking into account that the simulation parameters were not further refined in the quasi-3D simulations. The threshold currents of the a-SQW devices

were higher than those of the s-SQW lasers as a consequence of the lower optical confinement factor. The measured and simulated beam propagation ratios M^2 (defined using the $1/e^2$ criterion) for the 4º devices are shown in Fig. 3b). The experiments show an improvement of the beam quality for the asymmetric devices (lower M^2), confirming the predictions in ref. [16]. The best results were obtained in the 6º a-SQW device, with $M^2 < 2$ at 2 W.
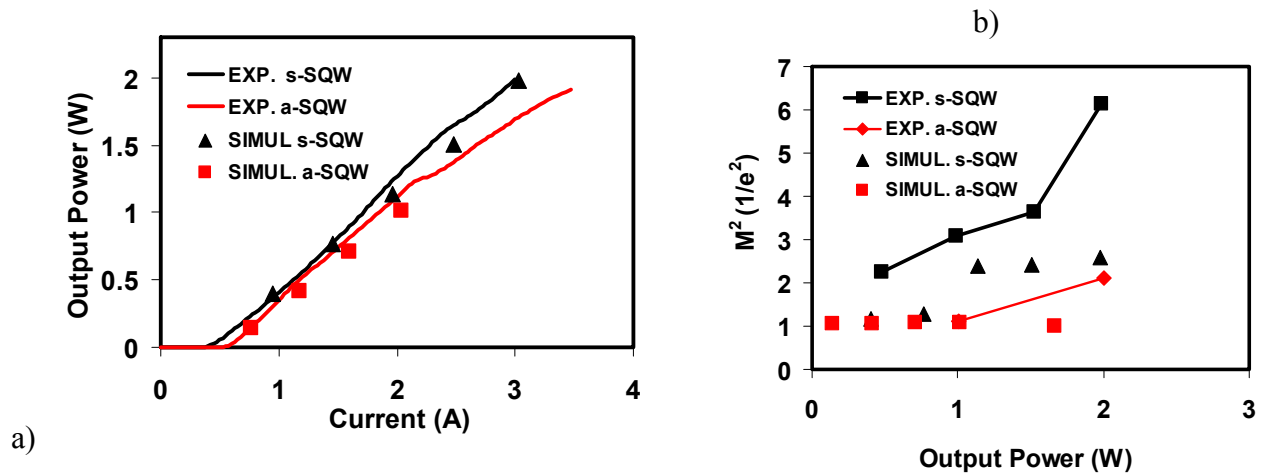

Fig. 3. Experimental and simulated power-current characteristics (a) and Beam Propagation ratio M^2 ($1/e^2$) (b) for 4º tapered lasers based on s-SQW and a-SQW epitaxial designs.

The beam properties predicted by the simulations were similar, although not identical, to the experiments. Fig. 4 compares, for a 4º a-SQW laser, the simulated and experimental profiles of the FF, NF at waist and NF at facet. This good agreement indicates that the main physical mechanisms responsible for the beam characteristics are considered in the model.
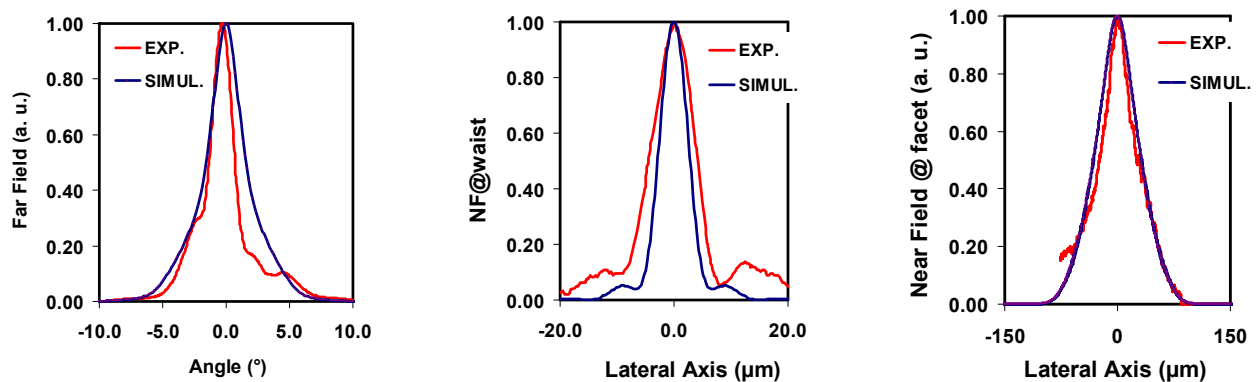

Fig.4. Experimental and simulated patterns of the FF (left), NF at waist (center) and NF at facet (right) for the 4º tapered laser based on the a-SQW epitaxial design at P = 1 W.

3.2   Role of thermal effects

As in any other high power semiconductor laser, thermal effects caused by self-heating are an important issue in the performance of tapered lasers. The role of thermal effects in the device characteristics is twofold: i) the overall heating of the device when driven in cw conditions decreases the modal gain, modifies the recombination rates (specially Auger recombination), and changes the internal distribution of carriers, producing an increase of the threshold current as in any other type of semiconductor laser; and ii) the lateral temperature profile induces a lateral index profile which changes the beam characteristics through the so-called thermal lensing effect. The second effect has been previously studied by numerical simulations in tapered amplifiers[19] and lasers[11,20]. Experimental results comparing cw and pulsed measurements in tapered lasers have been reported [11, 21, 22]. Previous experimental and simulated results indicate that the internal temperature profile in tapered lasers produces a positive thermal lensing effect, i.e., an increase of the self-

focusing caused by the carrier lensing. This effect manifests as an increase of the astigmatism with output power[20, 21, 22] in gain guided tapered lasers and as an increase of far-field broadening in index-guided tapered lasers[11].

Our initial simulations in 980 nm gain-guided tapered lasers[5] indicated that thermal effects can also produce a negative lensing effect, counteracting the positive carrier lensing effect. We have later simulated different types of tapered lasers at different wavelengths and we have compared the results obtained in isothermal and thermal (including self-heating) conditions. We observed that the simulated thermal profile can act as positive lens (convergent internal lens), negative lens (divergent internal lens) or neutral (minimum lensing), depending on the particular device geometry, internal parameters, and power levels. Furthermore, the simulations show that the behavior of the lensing effect is very sensitive to the value of non-well known internal parameters, such as the Auger recombination coefficient and the free-carrier absorption coefficient.

In order to get a physical understanding of the origin of the thermal lensing effect, we analyze in this work the role of thermal effects in 1060 nm gain guided tapered laser by comparing simulations performed in isothermal and thermal conditions with experiments performed in pulsed and cw conditions. In particular, we analyze the internal profiles of carrier density, temperature and refractive index.

The epitaxial structure corresponds to the s-SQW design described in section 3.1. The RW and tapered sections lengths were 0.7 and 3 mm, respectively, and devices with 4º and 6º taper angles were fabricated. AR (0.1%) and HR (95%) coatings were applied to the front and back facet, respectively. The p-side down mounted devices were characterized at room temperature in CW and pulsed (400 ns; 1 kHz) operation. Details on experimental results for the 4º devices can be found elsewhere[17].
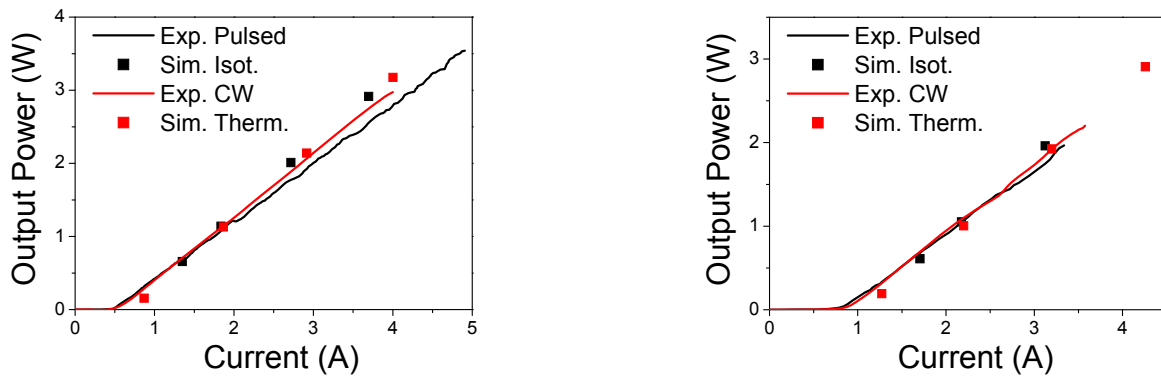

Fig. 5. Experimental and simulated power-current characteristics for 4º (left) and 6º (right) devices in pulsed and CW driving conditions.

Table 2: Experimental and simulated threshold currents and slope efficiencies for the 4º and 6º tapered lasers.

Taper angle	4º				6º			
Driving/simulation conditions	Pulsed/isother.		CW/thermal		Pulsed/isother.		CW/thermal	
	EXP.	SIM.	EXP.	SIM.	EXP.	SIM.	EXP.	SIM.
Threshold current (mA)	486	685	517	705	790	1065	858.7	1066
Slope Efficiency (W/A)	0.78	0.99	0.89	0.97	0.78	0.95	0.81	0.90

Fig. 5 shows a comparison between the experimental and simulated Power-Current characteristics. The values of the threshold currents and slope efficiencies are summarized in table 2. In general, the simulations reproduce quantitatively

the experimental results (within 10-20%), although the simulated threshold currents and slope efficiencies are higher than the experimental values. These differences are attributed to uncertainty in the value of the AR coating reflectivity. The experimental and simulated threshold currents in cw conditions are higher than those measured in pulsed operation or calculated without thermal effects, as expected, but the measured slope efficiencies are higher in cw than in pulsed conditions (see table 2).

The measured and simulated beam propagation ratios M^2 (defined using the $1/e^2$ criterion) for the 4º and 6º devices are shown in Fig. 6. The far-field divergence and width of the NF at waist, both defined at $1/e^2$, are shown in Fig. 7 for the 4º device. M^2 increases with the output power, and takes higher values in pulsed experiments and isothermal simulations than in cw experiments and thermal simulations, respectively. This unexpected behavior indicates that thermal lensing counteracts carrier lensing which is the main effect causing beam degradation. In any case, both experimental and simulated results show that thermal effects are not strongly relevant in the beam properties of these devices, as it can be confirmed by the relatively small differences in the beam parameters shown in Figs. 6 and 7.
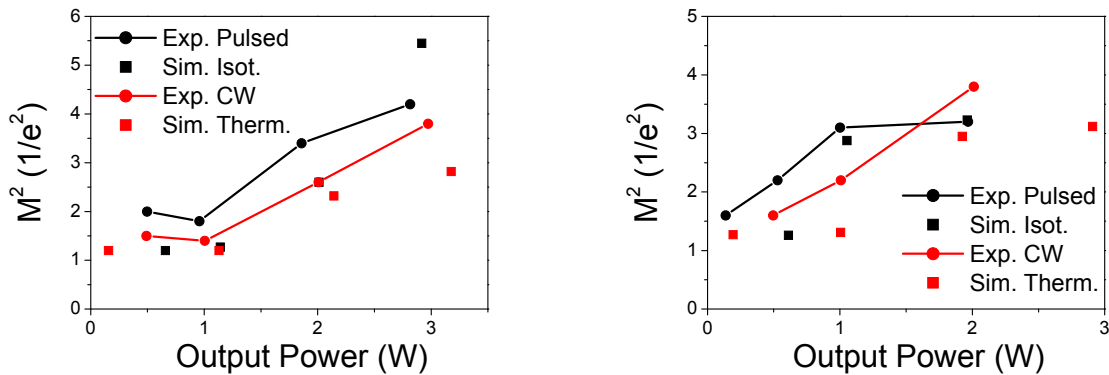

Fig. 6. Experimental and simulated evolution of beam propagation ratio M2 (1/e2) for 4º (left) and 6º (right) devices in pulsed and CW driving conditions.
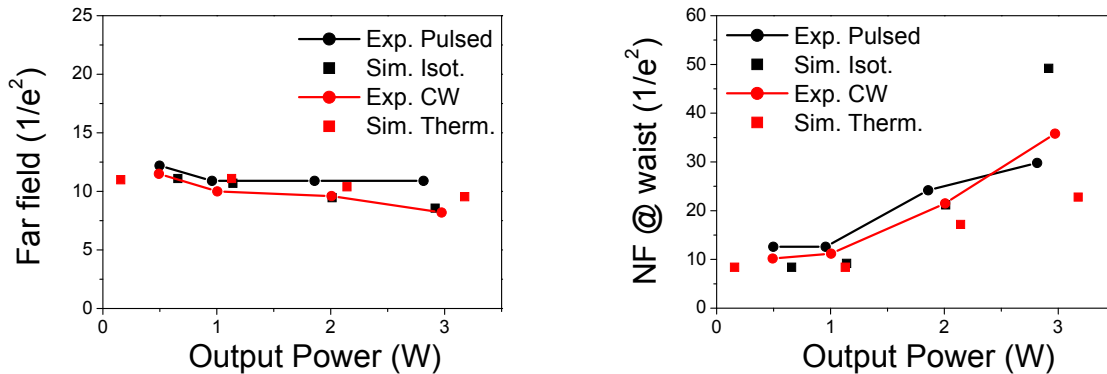

Fig.7. Experimental and simulated evolution of Far Field width (left) and Near Field at waist (right) for 4º devices in pulsed and CW driving conditions.

The good agreement observed between simulations and experiments indicates that the calculated internal temperature distribution can be used to analyze the role of self-heating in the beam properties of these tapered lasers.

It is well known that the strong non-uniformity of the photon density in the cavity of tapered lasers induces a depletion of carriers in the center of the cavity, the SHB effect. This effect is illustrated in Fig. 8, where we have plotted the calculated photon and carrier density distributions along the cavity at high output power (2 W). The carrier induced index profile produces a positive lensing effect which further confines the photons in the center of the cavity, triggering the beam self-focusing. This carrier lensing effect is illustrated in Fig. 9a, where we have plotted the NF patterns at facet at different powers, simulated in isothermal conditions in order to evaluate only carrier effects. The trend towards beam self-focusing can be inferred by the narrowing of the central part of the field at 2 W leading to a much narrower peak at 3 W. However, the self-focusing is lower when thermal effects are considered in the simulation as shown in Fig. 9b. This result indicates that thermal effects are opposite to carrier effects in this device, providing a negative lensing effect which defocuses the beam.
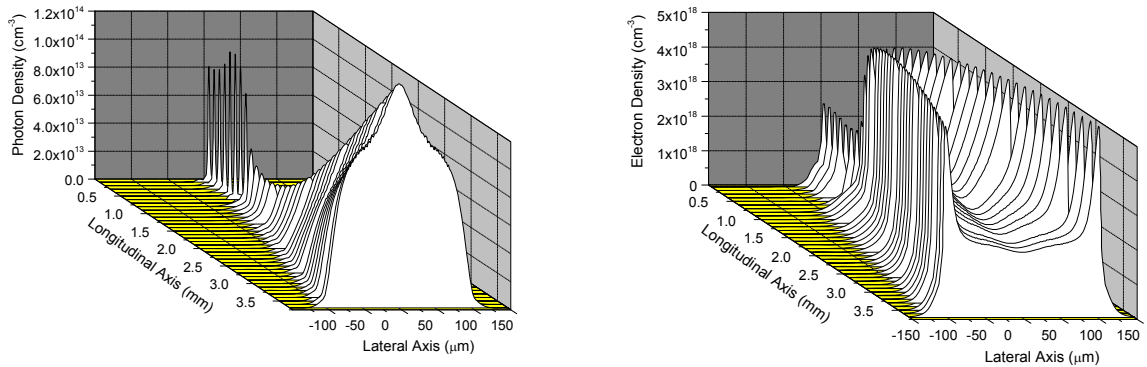

Fig. 8: Simulated photon density (left) and carrier density (right) profiles for 4º devices in thermal conditions at P = 2 W.
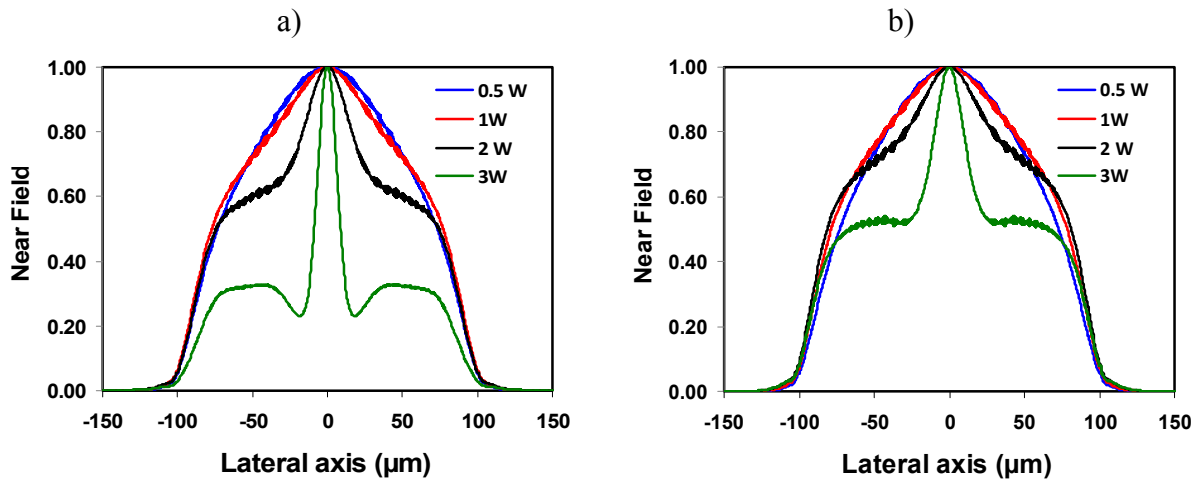

Fig. 9: Simulated Near Field patterns at facet for 4º devices in isothermal (a) and thermal (b) conditions.

The origin of the unexpected negative thermal lensing effect can be understood by considering the distribution of the local heat sources and the resulting temperature profile. As it has been described in more detail elsewhere[5, 13] our model considers the following non-uniform heat sources:

a) Joule heat: Proportional to the square of the current density and inversely proportional to the carrier concentration through the carrier conductivity; in general it hardly contributes to the global heating in properly designed laser structures.

b) Non-radiative recombination heat: Proportional to the Shockley-Read-Hall (SRH) and Auger recombination rates, and in consequence proportional to the addition of two terms, the first, an increasing function of the local carrier density (SRH recombination) and the second, proportional to the cube of the local carrier density (Auger recombination). In the case of SHB as in the tapered lasers, the non-radiative heat source profile shows peaks at the borders of the injected regions caused by the high carrier density in these regions.

c) Free-carrier absorption heat: Proportional to the product of the photon density and the carrier density, which in general results in a temperature distribution similar to that of photon density.

Therefore, the temperature profile along the lateral axis depends on the photon and carrier density profiles, as well as on the values of the recombination and free-carrier absorption parameters. Depending on the relative importance of the different heat sources, the final temperature profile in the tapered region can show a maximum at the cavity center caused by the photon density, two maxima at the borders of the injected regions caused by the carrier density maxima, and sometimes three maxima, caused by the addition of both effects.

Fig. 10 shows as an example the simulated temperature profile for the 4º tapered laser at high output power, $P = 2$ W. In the RW section ($z = 0$) the temperature distribution has a maximum at the cavity center, following the shape of the photon and carrier density profiles. In the tapered section (from $z = 0.7$ mm to 3.7 mm) the temperature is maximum at the sides of the injected region, due to the high carrier concentration in these zones (see Fig. 6) and to the corresponding high Auger recombination rate. The relative temperature minimum at the cavity center provides also a minimum in the temperature induced index perturbation, which counteracts the maximum of the carrier induced index perturbation. This behavior is illustrated in Fig. 9, where we have plotted the total index perturbation together with its temperature and carrier induced components at $z = 2$ mm. The guiding effect induced by the carriers is partly attenuated by the thermal antiguiding, explaining the lower self-focusing observed in the thermal simulations (Fig. 7) and the better beam quality observed experimentally in the cw measurements (Fig. 4).
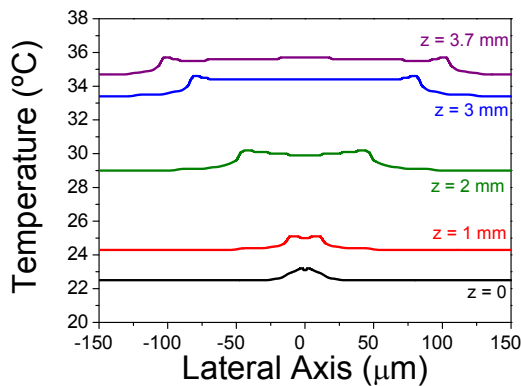

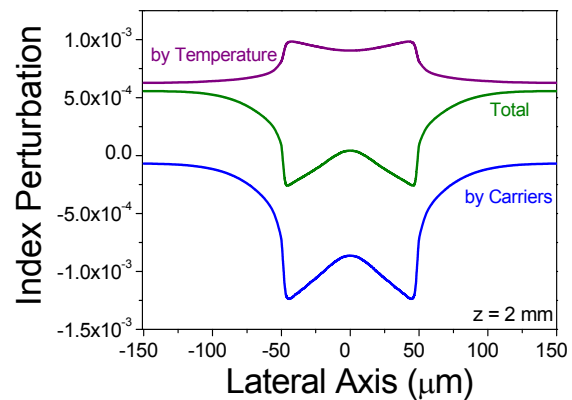Fig. 10: Simulated temperature profiles for 4º device at different longitudinal positions at P = 2 W.

Fig. 11: Simulated index perturbation profile along the lateral axis at z = 2mm (tapered region) for the 4º device at P = 2 W.

It is important to emphasize that the temperature induced antiguiding effect analyzed in this particular device is not a general behavior of tapered lasers; as previously commented positive thermal lensing has also been observed by other authors as well as by us in other tapered lasers. We just point out that the two opposite thermal effects are feasible, and that it is very difficult to determine a-priori which of the two trends will be dominant.

3.3 Tapered lasers with separate contacts

The use of tapered laser with separate contacts, where the current through the ridge waveguide (RW) section and the tapered section are separately controlled, is an interesting approach to improve the beam quality in cw operation[23] and also to provide the modulation of a high power laser beam with a small current excursion in the RW section[10]. In the second application an important parameter is the modulation efficiency, defined as the ratio between the increase of the output power when increasing the RW bias current, $\Delta P/\Delta I_{RW}$. We have previously reported a detailed analysis of the

improvement of beam quality in 980 nm tapered lasers with separate contacts[8] and have studied the design optimization of 1060 nm tapered lasers to achieve high modulation efficiency[24]. In this work we analyze the role of the epitaxial design on the properties of 1060 nm lasers with separate contacts, with the aim of understanding the experimental results.

The epitaxial structures are the s-SQW and a-SQW designs described in section 3.1. The RW and tapered sections lengths were 1 and 2 mm, respectively, and devices with 4º and 6º taper angles were fabricated, although we only present results for the 6º taper geometry. AR (2.5%) and HR coatings (95%) were applied to the front and back facet, respectively. The p-side up mounted devices were characterized at room temperature in CW operation using a constant drive current in the RW section.
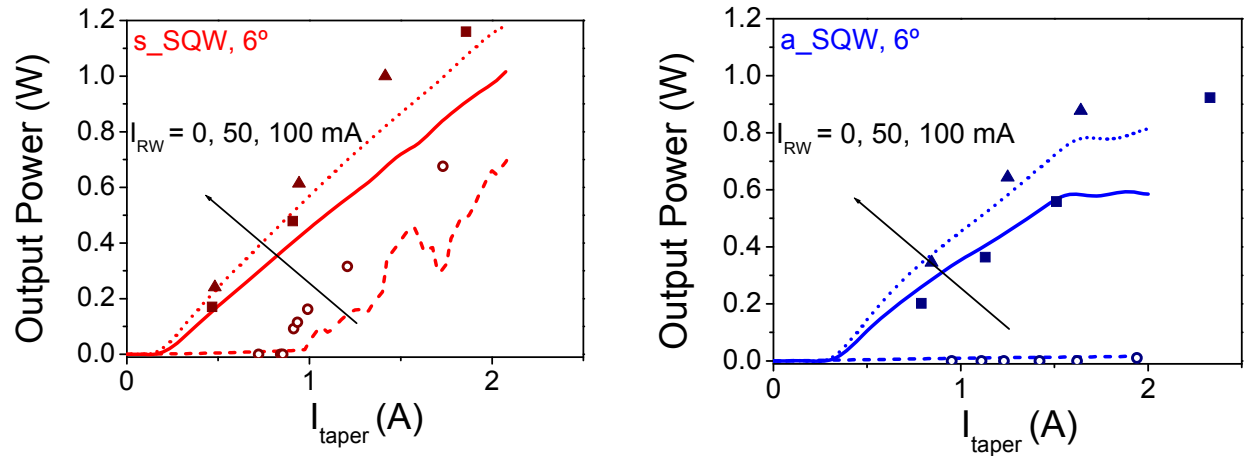

Fig. 12: Experimental (lines) and simulated (symbols) power-current characteristics for a s-SQW (left) and an a-SQW (right) 6º devices for different injection levels in the RW section (○ 0 mA; ■ 50 mA; ▲ 100 mA).

Fig. 12 shows a comparison between the experimental and simulated Power-Current characteristics for different injection levels in the RW section, I_{RW}. The values of the tapered section threshold currents at $I_{RW} = 0$ and $I_{RW} = 50$ mA are summarized in table 3. The simulations were performed using the same parameter set used for the tapered lasers reported in section 3.1, without further refinement. They show an excellent agreement with the experimental results in terms of threshold current at the different values of I_{RW}. The results in Fig. 12 show clear differences in the threshold current of the s-SQW and a-SQW structures, especially when comparing ΔI_{th}, defined as the difference between the tapered section threshold currents at $I_{RW} = 0$ and at $I_{RW} = 50$ mA. The tapered section threshold current for the s-SQW device at $I_{RW} = 50$ mA is around 1 A ($\Delta I_{th} \sim 0.8$ A) while for the a-SQW device it is higher than 2 A ($\Delta I_{th} > 1.6$ A), as the lasing condition was not reached below this current, neither in simulations nor in experiments. This indicates that a higher modulation efficiency can be obtained in the case of the a-SQW device, in this case 12 W/A. In consequence, the a-SQW device is, in what regards modulation efficiency, more suited for modulation applications than the s-SQW laser, although other considerations regarding switching speed and beam quality should be also taken into account.

Table 3: Experimental and simulated tapered threshold currents

Epitaxial structure	s-SQW		a-SQW	
	EXP.	SIM.	EXP.	SIM.
Taper Threshold current @ $I_{RW} = 50$ mA (A)	0.21	0.23	0.34	0.39
Taper Threshold current @ $I_{RW} = 0$ (A)	0.98	0.85	> 2	> 2

We have analyzed the origin of the differences between the s-SQW and a-SQW devices by means of a simple geometrical model. We consider the modal gain vs. current density characteristics of the two epitaxial designs shown in

Fig. 13. The QW material and dimensions are the same in both structures, and the difference arises from the different optical confinement factors, which is higher in the s-SQW. Using the geometrical area of the RW and tapered sections, we can estimate the contribution of both sections to the total gain at different injection levels, by considering that the total modal gain of the two section tapered laser g_{tot} can be expressed as:

$$g_{tot} = g_{RW}\left(\frac{L_{RW}}{L_{RW} + L_{tap}}\right) + g_{tap}\left(\frac{L_{tap}}{L_{RW} + L_{tap}}\right) \tag{1}$$

where g_{RW} (g_{tap}) and L_{RW} (L_{tap}) are the gain and length, respectively, of the RW (tapered) section. The calculated total gain for both structures at $I_{RW} = 0$ and $I_{RW} = 50$ mA are shown in Fig. 14. At threshold the total gain must equal the total cavity losses, which include the mirror, internal and geometrical losses of the unstable cavity. The calculated total losses are indicated by the horizontal line in Fig. 14, and then the estimated threshold currents are given by the intersections of the horizontal line with the total gain curves. In the case of $I_{RW} = 0$ the RW section is in absorbing conditions and therefore contributes with a negative gain, causing a lower modal gain at constant taper section current, and the observed higher threshold current, as it is indicated by the vertical lines in Fig. 14. The lower modal gain in the a-SQW lasers and the saturation of the gain in the tapered region explain the observed differences in ΔI_{th}, highlighted in the figure.
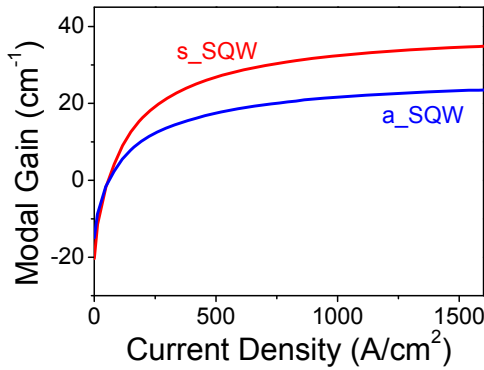

Fig. 13: Calculated modal gain vs current density characteristics for the s-SQW and a-SQW epitaxial designs.
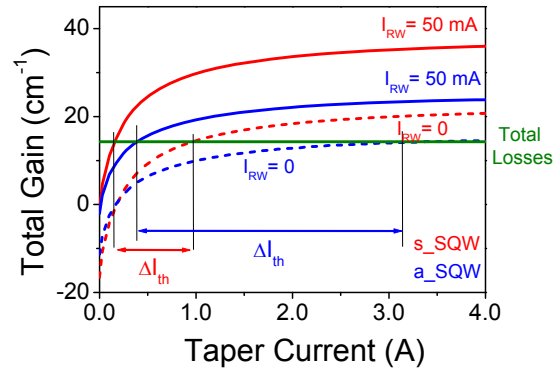
Fig. 14: Calculated total modal gain vs taper current characteristics for the s-SQW and a-SQW epitaxial designs at $I_{RW} = 0$ and $I_{RW} = 50$ mA. The horizontal line shows the total losses.

4. CONCLUSIONS

We have shown that a steady state single frequency Quasi-3D simulator for tapered lasers is a valuable tool to reproduce experimental results, to assess the design of new epitaxial structure and device geometries, and to analyze the internal physical processes in the unstable laser cavity.

The experimental results in 1060 nm tapered lasers confirm the simulation based predictions of an improvement in the beam quality in the case of asymmetric laser structures in comparison with symmetric devices, due to the reduced tendency to self-focusing. We have shown experimental and simulation results where thermal effects reduce the self-focusing caused by the carriers. The analysis of the results indicates that the local heat caused by non-radiative recombination is responsible for the negative thermal lensing effect. Finally, we have simulated and analyzed the properties of 1060 nm tapered lasers with separate contacts in comparison with experiments. We have found that the devices based on an asymmetrical epitaxial design are more suited to obtain high modulation efficiency due to the higher linear gain saturation.

ACKNOWLEDGMENTS

REFERENCES

[1] Walpole J. N., "Semiconductor amplifiers and lasers with tapered gain regions," Opt. Quantum Electron. 28, 623-645 (1996).

[2] Wenzel H., Sumpf B., Erbert G., "High-brightness diode lasers," C. R. Physique 4, 649-661 (2003).

[3] Sumpf, B., Hasler, K.-H., Adamiec, P., Bugge, F., Dittmar, F., Fricke, J., Wenzel, H., Zorn, M., Erbert, G., and Trankle, G., "High-Brightness Quantum Well Tapered Lasers". IEEE J. Selected Topics Quantum Electron. 15(3), 1009-1020 (2009).

[4] C. Fiebig, G. Blume, M. Uebernickel, D. Feise, C. Kaspari, K. Paschke, J. Fricke, H. Wenzel, y G. Erbert, "High-Power DBR-Tapered Laser at 980 nm for Single-Path Second Harmonic Generation". IEEE J. Select. Topics Quantum Electron. 15(3), 978-983, (2009).

[5] Borruel L., Sujecki S., Esquivias, I., Wykes, J., Sewell, P., Benson, T.M., Larkins, E. C., Arias, J., and Romero, B., "Selfconsistent Electrical, Thermal and Optical Model of High Brightness Tapered Lasers", Proc. SPIE 4646, 355-366 (2002).

[6] Borruel L., Sujecki S., Moreno P., Wykes J., Krakowski M., Sumpf B., Sewell P., Auzanneau S.C., Wenzel H., Rodríguez D., Benson T.M., Larkins E.C., Esquivias I., "Quasi-3-D Simulation of High-Brightness Tapered Lasers". IEEE J. Quantum Electron. 40, 463-472 (2004).

[7] Sujecki S., Borruel L., Wykes J., Moreno P., Sumpf B., Sewell P., Wenzel H., Benson T.M., Erbert G., Esquivias I., Larkins E.C., "Nonlinear Properties of Tapered Laser Cavities". IEEE J. Select. Topics Quantum Electron. 9, 823-834 (2003).

[8] Odriozola, H., Tijero, J. M. G., Borruel, L., Esquivias, I., Wenzel, H., Dittmar, F., Paschke, K., Sumpf, B. and Erbert, G., "Beam Properties of 980 nm Tapered Lasers with Separate Contacts: Experiments and Simulations", IEEE J. Quantum Electron. 45(1), 42 - 50 (2009).

[9] Borruel, L., Esquivias, I., Moreno, P., Krakowski M., Auzanneau, S.C., Calligaro, M., Parillaud, O., Lecomte, M., Sujecki, S., Wykes, J., Larkins, E.C., "Clarinet laser: Semiconductor laser design for high-brightness applications", Appl. Phys. Lett., 87, 101104 (2005).

[10] Michel, N., Odriozola, H., Kwok, C.H., Ruiz, M., Calligaro, M., Lecomte, M., Parillaud, O., Krakowski, M., Xia, M., Penty, R.V., White, I. H., Tijero J.M.G., and Esquivias, I., "High modulation efficiency and high power 1060 nm tapered lasers with separate contacts", Electron. Lett. 45(2), 103–104 (2009).

[11] Williams, K. A., Penty, R. V., White, I. H., Robbins, D. J., Wilson, F. J., Lewandowski, J. J. and Nayar, B. K., "Design of High-Brightness Tapered Laser Arrays", IEEE J. Select. Topics Quantum Electron. 5, 822-831 (1999).

[12] Mariojouls, S., Margott, S., Schmitt, A., Mikulla, M., Braunstein, J., Weimann, G., Lozes, F., Bonnefont, S., "Modeling of the Performance of High-Brightness Tapered Lasers", Proc. SPIE 3944, 395-406 (2000).

[13] Harold™ Reference Manual, Photon Design, Oxford (UK).

[14] Esquivias, I., Odriozola, H., Tijero, J. M. G., Mínguez, A. M. and Borruel, L., "A Self-Consistent CW Model of Unstable Cavity Semiconductor Lasers including Symmetrical and Antisymmetrical Solutions", Bragg Gratings, Photosensitivity and Poling in Glass Waveguides/ Nonlinear Photonics on CD-ROM (The Optical Society of America, Washington, DC, 2007), JWA5.

[15] Guthre, J., Tan, G. L., Ohkubo, M., Fukushima, T., Ikegami, Y., Ijichi, T., Irikawa, M., Mand, R. S. and Xu, J. M., "Beam instability in 980 nm power laser: Experiment and analysis," IEEE Photon. Technol. Lett. 6(12), 409-1411 (1994).

[16] Tijero, J. M. G., Odriozola, H., Borruel, L., Esquivias, I., Sujecki, S. and Larkins, E. C., "Enhanced Brightness of Tapered Laser Diodes Based on an Asymmetric Epitaxial Design," IEEE Photonics Technol. Lett. 19, 1640-1642 (2007).

[17] Ruiz, M., Odriozola, H., Kwok, C.H., Michel, N., Calligaro, M., Lecomte, M., Parillaud, O., Krakowski, M., Tijero, J. M.G., Esquivias, I., Penty, R.V. and White, I.H., "High-brightness tapered lasers with an Al-free active region at 1060 nm", Proc. SPIE 7230, 72301D (2009)

[18] Odriozola, H., Tijero, J. M. G., Esquivias, I., Borruel, L., Martin-Minguez, A., Michel, N., Calligaro, M., Lecomte, M., Parillaud, O., Krakowski, M., "Design of High-Brightness Tapered Lasers at 1060 nm Based on an Asymmetric Al-free Active Region Structure," IEEE PhotonicsGlobal@Singapore, IPGC 2008, 1-4 (2008).

[19] Lang, R. J., Hardy, A., Parke, R., Mehuys, D., O'Brien, S., Major, J., Welch, D., "Numerical analysis of flared semiconductor laser amplifiers," IEEE J. Quantum Electron. 29 (6), 2044-2051 (1993).

[20] Marijolous S., S. Morgott, A., Schmitt, M., Mikulla, J. Braunstein, G.Weimann, "Modeling of the performance of high-brightness tapered lasers," Proc. SPIE 3944, 395-406 (2000).

[21] Schmitt, A.; Mikulla, M.; Walther, M.; Kiefer, R.; Braunstein, J.; Weimann, G., "Stability of the beam quality of 0.98-µm InGaAlAs tapered laser oscillators," Proc. CLEO/Pacific Rim '99 4, 1097 - 1098 (1999).

[22] Jensen, O. B., Klehr, A., Dittmar, F., Sumpf, B., Erbert, G., Andersen, P. E., and Petersen, P.M., "808 nm tapered diode lasers optimised for high output power and nearly diffraction-limited beam quality in pulse mode operation", Proc. SPIE 6456, 64560A (2007).

[23] Paschke, K., Sumpf, B., Dittmar, F., Götz, E., Staske, R., Wenzel H. and Tränkle, G., "Nearly Diffraction Limited 980-nm Tapered Diode Lasers With an Output Power of 7.7 W," IEEE J. Select. Topics Quantum Electron. 11, 1223-1227 (2005).

[24] Odriozola, H., Tijero, J. M.G., Esquivias, I., Borruel, L., Martín-Mínguez, A., Michel, N., Calligaro, M., Lecomte, M., Parillaud, O. and M. Krakowski., "Design of 1060 nm Tapered Lasers with Separate Contacts," Opt. Quantum Electron. 40(14-15), 1123-1127 (2008).